

Personalized On-line Adaptation of Kinematic Synergies for Human-Prosthesis Interfaces

Ricardo Garcia-Rosas, Ying Tan, Denny Oetomo, Chris Manzie, and Peter Choong

Abstract—Synergies have been adopted in prosthetic limb applications to reduce complexity of design, but typically involve a single synergy setting for a population and ignore individual preference or adaptation capacity. In this paper, a systematic design of kinematic synergies for human-prosthesis interfaces using on-line measurements from each individual is proposed. The task of reaching using the upper-limb is described by an objective function and the interface is parameterized by a kinematic synergy. Consequently, personalizing the interface for a given individual can be formulated as finding an optimal personalized parameter. A structure to model the observed motor behavior that allows for the personalized traits of motor preference and motor learning is proposed, and subsequently used in an on-line optimization scheme to identify the synergies for an individual. The knowledge of the common features contained in the model enables on-line adaptation of the human-prosthesis interface to happen concurrently to human motor adaptation without the need to re-tune the parameters of the on-line algorithm for each individual. Human-in-the-loop experimental results with able-bodied subjects, performed in a virtual reality environment to emulate amputation and prosthesis use, show that the proposed personalization algorithm was effective in obtaining optimal synergies with a fast uniform convergence speed across a group of individuals.

Index Terms—Upper limb prosthetics; synergy-based prosthesis interface; grey-box on-line optimization; coordinated prosthesis control; human-in-the-loop.

I. INTRODUCTION

In order to accommodate human-to-human physiological and motor control variations, and the numerous variations in the nature of amputation [1], personalization of Human Prosthesis Interfaces (referred to as HPIs henceforth) is a necessary and critical step in realizing the effective operation of a prosthesis [2]. Take for instance synergistic HPIs, where motion of a powered prosthesis is driven in coordination with the motion of the residual limb [3]. Kinematic synergies in HPIs have been actively studied in recent years due to their potential to realize coordinated motion of the multiple degrees of freedom (DOF) in the human-prosthesis limb, as required by activities of the daily living [4], [5]. Despite its potential, the need for personalization has been explicitly identified for this interface modality due to the high degree of person-to-person variations in motor preferences and behavior [6].

Recent studies have investigated the kinematic synergy-based HPI strategies mostly through an artificial neural network based approach, by using the data gathered from able-bodied subjects to train the algorithms [7], [8], [9], [10].

This project is funded by the Valma Angliss Trust.

R. Garcia-Rosas, Y. Tan, D. Oetomo, and C. Manzie are with the School of Electrical, Mechanical and Infrastructure Engineering, and P. Choong with the Department of Surgery, The University of Melbourne, VIC 3010, Australia. ricardog@student.unimelb.edu.au; [yingt,doetomo,manziec,pchoong}@unimelb.edu.au](mailto:{yingt,doetomo,manziec,pchoong}@unimelb.edu.au).

This yields the interface setting that best fits the population from which the training data-set was created. However, given individual variations in motor preferences, capabilities and the effect of motor learning, as well as the more significant changes due to amputation, these interfaces needed to be systematically personalized to be effective for amputees [6].

In [11], different techniques of linear regression were performed in a bid to obtain a common synergy for a set of able-bodied people. The identified synergy setting was then used on individual emulated amputees. This study concluded that the choice of regression technique did not significantly improve the performance of the synergistic prosthetic interface. The results in [11], however, demonstrated that while general common motor features can be observed (a general trend in limb trajectory), there is also a significant amount of inter-subject variability. These results justify the need for personalization of kinematic synergies in HPIs, which has not been addressed to date.

If the synergy is kept constant, the individual will learn that particular setting while using the device. This constant setting may not be the optimal for that individual. In order to find the optimal setting for a particular individual, the process of personalization needs to evaluate the individual's performance at a range of settings until the optimal setting is identified. Performing this personalization procedure concurrently to the individual learning to use the prosthesis through a process of on-line adaptation is advantageous as it can reduce the time needed to identify the optimal setting for an individual. While there are a plethora of data-driven techniques that adapt system parameters in accordance with [12], [13], optimizing synergies in a HPI setting offers additional challenges as observed in [14], [15]. This has also been attempted in lower limb prosthetics [16].

A significant challenge to the on-line personalization of HPIs is due to human motor learning, as the individual learns and adapts following a change in synergy. This learning behavior introduces transient dynamics to task performance in the iteration domain. Hence the mapping between the performance and parameterization can only be obtained after steady-state in iteration domain is reached. This could take a long time and many iterations of the task, which the personalization algorithm would need to wait for; thus making the algorithm impractical. Furthermore, different individuals have different transient learning characteristics, such that the minimum time for any individual to reach their optimal performance using a given synergy setting is not known in advance. Because of this, tuning of the personalization algorithm to each individual is impractical. An example of this particular challenge is presented in Figure

1, where the on-line personalization algorithm in [15] was tuned to identify the synergy for subject A. The resultant personalization process for subject A is shown on the left side of the figure, where the subject's performance and the synergy setting are shown across iterations of the task. Clear convergent behavior can be observed in both metrics for subject A. The same algorithm tuning was then applied to another individual, subject B. The resultant personalization process for subject B is shown on the right side of Figure 1, where undesirable behavior indicated by high variability in performance and apparent lack of convergence in the synergy can be observed. It may be concluded that a lack of personalized algorithm tuning resulted in failure to personalize the synergy for subject B. Finally, as each individual has an unique input to steady-state output mapping, the gradientbased algorithm presented in [15] is not able to achieve unified convergence performance across the population.

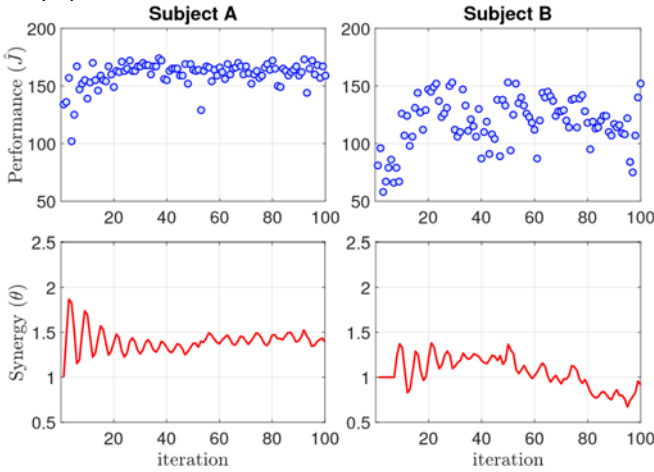


Fig. 1. Experimental implementation of algorithm in [15] results for performance and synergy for two subjects. Performance was given by a combination of completion time and accuracy of a reaching task. The algorithm was tuned specifically for subject A and applied to both subjects. The top plots show performance across iterations while the bottom plots show synergy across iterations.

In this paper, a method that enables the personalization of HPIs to operate concurrently to the individual learning to use the prosthetic device is proposed. This is done through the formalization of the observed common features in motor behavior via a grey-box model. The model captures the observed common motor features in its structure, and individual variations in its parameters. Through this model, specific properties of the structure of the human-prosthesis system are identified. Using the knowledge of these properties, an extremum seeking based algorithm [17], [18] is adapted to the HPI application, such that its tuning parameters are insensitive to human variations and fast uniform convergence across a population can be achieved. Providing the means for the online personalization of kinematic synergies for HPIs to be performed without the need for individuals to reach steady-state in task performance.

The following notation is used throughout the paper. The set of real numbers is denoted as \mathbb{R} , the set of positive real numbers is denoted as \mathbb{R}^+ . The term “synergy” is used to describe the parametrization of the human-prosthesis

interface. For a given static mapping $y_x = h(x) : \mathbb{R} \rightarrow \mathbb{R}$, its gradient is expressed as $y_x = \partial h(x)/\partial x$, and curvature (Hessian) as $y_{x^{00}} = \partial^2 h(x)/\partial x^2$. The subscript x_i is used to indicate the iteration domain, such that x_i indicates the i th iteration of x . The “bar” notation on a variable, e.g. $\bar{\lambda}$, indicates that the variable is individual dependent.

II. HUMAN MOTOR PREFERENCE AND ADAPTATION MODEL

In this section, the common features observed in motor behavior for individuals using a HPI based on kinematic synergies are discussed and their formalization within a greybox model is proposed.

A. Common features in human motor behavior

It has been demonstrated that by characterizing an upperlimb reaching task, using a synergistic prosthesis, by an objective function and by parameterizing the HPI two common motor features arise [14]. There exists a non-linear steady-state input-output relationship between synergies and a characterization of the task as an objective function (performance). This relationship is dependent on the formulation of the objective function and can be made to have an extremum [14]. Let the measured performance of the task be characterized by the performance $\hat{J}_i \in \mathbb{R}^+$. Let the parametrization of the interface, or synergy, be given by $\theta_i \in \Theta$, where Θ is a compact set in \mathbb{R} representing the parameter set of interest.

Measured performance is explicitly defined using the following objective function:

$$\hat{J}_i(\theta) = \frac{0.25 \|\bar{\mathbf{p}}_{fmax}\|^2}{\max(0.25, \|\bar{\mathbf{p}}_{f,i}\|^2)} + \frac{16.67 t_{fmax}}{\max(0.5, t_{f,i})}. \quad (1)$$

Here, $\bar{\mathbf{p}}_{f,i}$ is the hand end position error from target, and $\bar{\mathbf{p}}_{fmax} = 10\text{cm}$; $t_{f,i}$ is the reach time; and $t_{fmax} = 3\text{s}$. Note that both $\bar{\mathbf{p}}_{f,i}$ and $t_{f,i}$ are influenced by θ and $\hat{\mathbf{q}}_r$, where $\hat{\mathbf{q}}_r$ is the angular velocity of the residual limb.

An example of the relationship between the synergy (θ) and performance (\hat{J}) is shown in Figure 2. An individual's average performance over multiple iterations of the task for a range of synergy values conforms an Input-to-Steady-State-Output (ISSO) map whose extremum and shape differs across individuals. This individual variation in best performing parameter suggests the existence of preference in the configuration of the prosthetic interface. The shape of this average map for individuals has been identified as the common feature while the parameters that define the map and its extremum as individual variations. In this work, this average map feature will be referred to as “motor preference”.

Furthermore, a transient behavior was observed in performance as the synergy setting was changed from one value to the next, where the dynamics are individual dependent. As expected from human behavior, the performance across iterations of the task is affected by the variability inherent in human motor control [19]. An

example of this transient behavior is presented in Figure 3. In this work, this transient dynamics feature will be referred to as “motor adaptation”. This type of transient learning behavior has been extensively

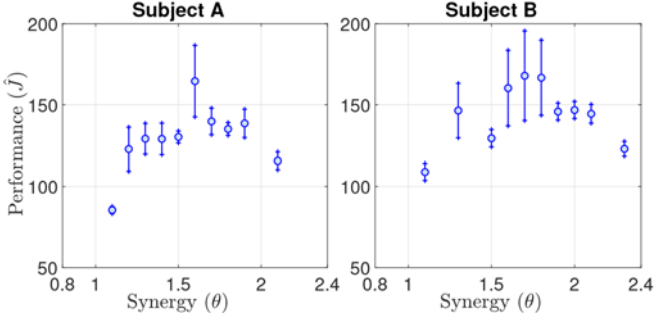


Fig. 2. Experimentally obtained synergy-performance map for two representative subjects. The blue circles represent mean performance while the whiskers the standard deviation. Task performance was characterized by a quadratic-like objective function, while synergy represents a kinematicsynergy parametrization of the human-prosthesis interface.

modeled in the literature, with state-space models, exponentially decaying responses, and Linear Time Invariant (LTI) with output additive Gaussian white noise being widely accepted, e.g. [20], [21], [22], [23], [24]. Although many models have been developed to characterize motor adaptation in able-bodied individuals, a direct link to the prosthetic case is yet to be established. It is worthwhile to highlight that the motor adaptation observed in Figure 3 captures the learning of a given objective function for a task by repetition, i.e. iteratively. The observed behavior suggests that a transient response in the iteration domain has a common structure and individual dependent parameters.

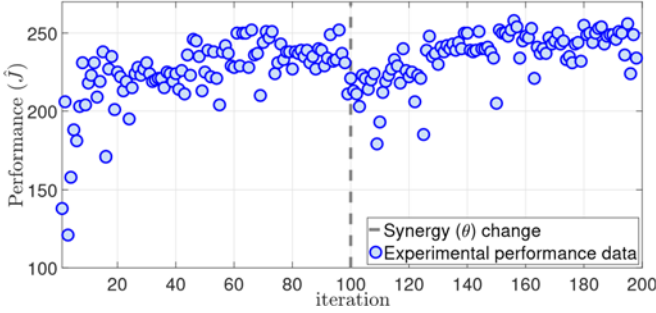


Fig. 3. Experimentally obtained performance across iterations data for two synergy values for a representative subject. The dashed line represents the change in the value of the kinematic-synergy parametrization (synergy) of the human-prosthesis interface. Performance was characterized by a quadratic-like objective function.

The proposed model for an individual’s performance as a function of the synergy is constructed by the serial combination these two features: the average non-linear convex map (motor preference) and a perturbed LTI system in the iteration domain (motor adaptation). Figure 4.(A) shows the diagram of the proposed model. Figure 4.(B) shows the combined human-prosthesis system whose performance as a function of the synergy is being captured by the model. Although there exist models that incorporate transient motor learning behavior in the iteration domain [23], to the best of the authors’ knowledge, a model that incorporates both preferences in motor behavior and

individual transient learning behavior is novel in the literature.

The steady-state relationship between synergy and performance in the model represents the measured synergyperformance I-SSO map obtained experimentally as presented in Figure 2. The scalar v_i characterizes human motor performance variation. $u_{\theta,i} \in \mathbb{R}$ is the output of the average static map representing motor preference. $y_i \in \mathbb{R}$ is the output of the LTI system representing motor adaptation, which introduces transient dynamics to the average static map. This represents the internal cost, which is subsequently approximated using \hat{J}_i from (1).

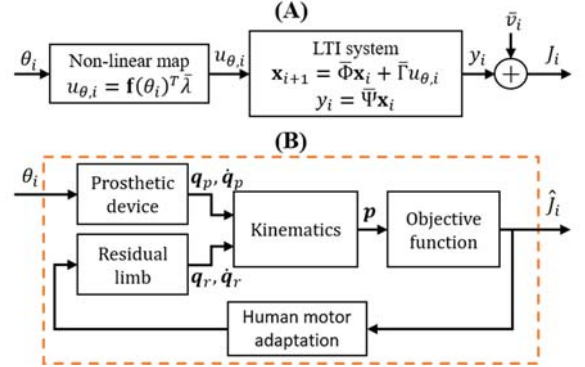


Fig. 4. Overview of proposed human motor preference and adaptation model. (A) The grey-box model composed of a non-linear map and a LTI system in the iteration domain. (B) The block diagram of the human-prosthesis system represented by the model, as per the characterization of the task through an objective function (\hat{J}_i) and a parametrization of the prosthetic interface (θ_i).

B. Motor preference

Given the average I-SSO relationship observed experimentally [14], motor preference is then modeled as a non-linear static input-output map. This map can be represented in general by a linearly-parameterized non-linear function

$$u_{\theta,i} = \mathbf{f}(\theta_i)^T \bar{\lambda}, \quad (2)$$

where $\mathbf{f}(\cdot) : \Theta \rightarrow \mathbb{R}^n$ is the vector of continuously differentiable characterizing functions, which is common across a population. And $\bar{\lambda} \in \mathbb{R}^n$ is a constant vector of parameters, which is individual dependent. In this case $u_{\theta,i}$ represents the average performance for a given θ_i . The synergy θ_i is the current setting of the parametrization of the HPI and is considered as an input to the non-linear mapping.

Remark 1. In the approach proposed herein, $\mathbf{f}(\cdot)$ is considered to be a common basis across a broad population, whilst the individual preferences are captured in the parameter vector $\bar{\lambda}$.

The following assumption is considered regarding the characterization of motor preference.

Assumption 1. There exists a unique maximum $\theta^ \in \Theta$ such that for any given $\bar{\lambda} \in \mathbb{R}^n$, there is $u^*_{\theta} = \mathbf{f}(\theta^*)^T \bar{\lambda}$, $\theta^* \in \Theta$, and*

$$u'_{\theta}(\theta) = 0, \quad \text{iff } \theta = \theta^*, \quad (3a)$$

$$u''_{\theta}(\theta) < 0, \quad \forall \theta \in \Theta. \quad (3b)$$

Remark 2. Assumption 1 can be satisfied by carefully formulating the interface parametrization and measure of task performance, as previously presented in [14]. Although u^* depends on the parameter $\bar{\lambda}$, the optimal parameter θ^* is independent of the parameter $\bar{\lambda}$. From experimental results [14], it was observed that individuals who reached steady state task performance with a virtual synergistic prosthetic device satisfy this assumption locally, as seen in Figure 2. ◦

C. Motor adaptation

A model to characterize the transient behavior observed in performance (J) as the synergy setting (θ) changed from one value to the next, which can be attributed to motor adaptation, is presented next. In this work, due to repetitive nature of the tasks being considered, a Linear Time-Invariant (LTI) state-space model in the iteration domain is utilized to represent human learning behavior. Human motor variation is represented as additive noise with respect to the given performance. Such representation is natural to represent the experimental and application setting as performance over one iteration of the task is used as an output. At the i^{th} iteration, the proposed model takes the following form:

$$\mathbf{x}_{i+1} = \bar{\Phi}\mathbf{x}_i + \bar{\Gamma}u_{\theta,i} \quad (4a)$$

$$J_i = \bar{\Psi}\mathbf{x}_i + \bar{v}_i \quad (4b)$$

where $\mathbf{x} \in \mathbb{R}^{n_h}$ represents the internal states of human motor adaptation and $n_h > 0$ is the order of the model. The matrices $\bar{\Phi}$, $\bar{\Gamma}$, and $\bar{\Psi}$ have the appropriate dimensions and are individual dependent. Performance is perturbed by human motor variation, which is represented by the output additive noise \bar{v} [20]. An example of the observed motor adaptation behavior is presented in Figure 3. The following assumption is considered:

Assumption 2. System (4) has unity steady-state gain

$$(G_{ss} := \bar{\Psi} (I_n - \bar{\Phi})^{-1} \bar{\Gamma} = 1). \quad \circ$$

Remark 3. Assumption 2 allows the map $u_{\theta,i}$ (2) to represent an individual's average static relationship between synergy (θ) and performance (J). This can be readily satisfied through the selection of $\bar{\lambda}$. ◦

D. Model validation

In order to validate the proposed model structure, system identification was performed on synergy-performance data for two representative subjects and the simulation of the identified systems was compared to a different synergy-performance data-set from these individuals. The identification procedure is as follows: first, the data collected is used to identify the parameters of the non-linear I-SSO map, followed by the identification of the normalized LTI system. Finally, the characteristics of motor performance variation (\bar{v}_i) are obtained from the analysis of residuals between the validation data and the identified underlying model.

The dataset for the two individuals used for system identification was taken from the authors' previous work in

[14] and a new dataset from the same individuals was generated for comparison with the identified model and validation. The original dataset was generated by holding a synergy constant over multiple iterations of a forward reaching task with a synergistic prosthetic elbow. This procedure was followed in order to capture both the transient and steady-state behavior for each synergy. This was repeated for multiple synergies to obtain the non-linear map. The validation dataset was generated with the same task and subjects, however, the synergy was changed linearly in every task iteration instead; capturing both features in the response.

1) Average I-SSO map: In order to identify the I-SSO map, the structure of $\mathbf{f}(\theta)$ is needed. As in [14], the nonlinear mapping was approximated as a quadratic polynomial. The linearly parameterized non-linear function representing motor preference is given by

$$J(\theta) = u_{\theta,ss}(\theta) = \mathbf{f}(\theta)^T \bar{\lambda} = [\theta^2 \quad \theta \quad 1] \bar{\lambda}, \quad (5)$$

with $\bar{\lambda} \in \mathbb{R}^3$ being the parameters identified for each individual. The map was identified from experimental data using a least squares method. Figure 5 shows the identified $J(\theta)$ map for two subjects using a quadratic polynomial along with the experimental data used for identification. The identified map parameters $\bar{\lambda}$ for both subjects are the following.

$$\bar{\lambda}_A = [-158.15 \quad 529.18 \quad -293.34]^T, \quad (6a)$$

$$\bar{\lambda}_B = [-96.18 \quad 342.13 \quad -147.86]^T. \quad (6b)$$

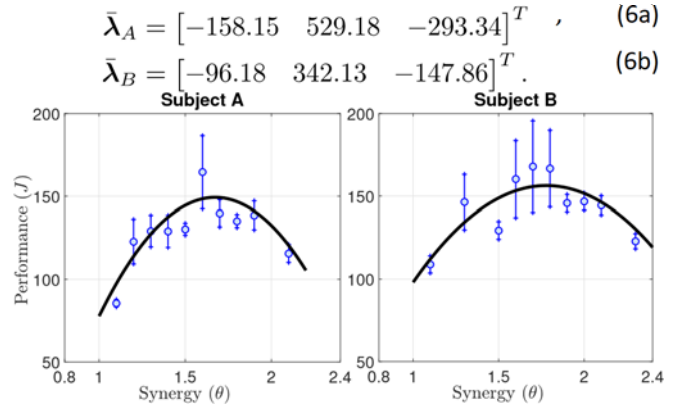


Fig. 5. Non-linear map observed experimentally with quadratic fit for two representative subjects. The blue circles represent mean performance, the whiskers the standard deviation, and the black line the quadratic polynomial representing the identified map.

2) Normalized LTI system: There are two components in (4) that need to be identified in order to characterize an individual's learning dynamics: the underlying LTI model and the associated noise (\bar{v}). Undershoot in performance has been observed to occur following step synergy changes, as illustrated in Figure 3. This can be attributed to the individual's reduced performance due to the sudden change in the synergy setting applied and the gradual re-adaptation to the dynamics of the new synergy setting. Thus, systems of order greater than one are considered for identification, as these are the minimum required to capture undershoot. Furthermore, as overshoot is non-physical in the timescales considered, constrained least squares was used for identification in order to limit the identified systems to be over-damped. The identified non-linear I-SSO map from the

previous section was used as the input u_θ to the LTI subsystem.

The experimental data for the transient response corresponding to a single synergy value was used for validation of the identified LTI system. Validation was performed through the comparison of the Mean Square Error (MSE) between the response of the identified underlying model and the validation data-set for different system orders [13]. Table I contains the resultant MSE for the second and third order cases for both subjects.

As seen in the validation results presented in Table I, both the second and third order models achieve similar MSE. Since it is desirable to use the lowest complexity model, and the

TABLE I

MEAN SQUARE ERROR (MSE) FOR THE SECOND AND THIRD ORDER LTI SYSTEM MODELS.

Subject	2nd order MSE	3rd Order MSE
A	277.76	274.36
B	489.93	467.37

second order model captures the key transient behavior, the second order model is selected. The identified normalized LTI system matrices representing the underlying individual transient behavior for subjects A and B are listed below.

$$\bar{\Phi}_A = \begin{bmatrix} 0 & 1 \\ 0.068 & 0.35 \end{bmatrix}, \quad (7a)$$

$$\bar{\Gamma}_A = [0.839 \ 0.037]^T, \bar{\Psi}_A = [1 \ 0], \quad (7b)$$

$$\bar{\Phi}_B = \begin{bmatrix} 0 & 1 \\ -0.017 & 0.25 \end{bmatrix}, \quad (8a)$$

$$\bar{\Gamma}_B = [-0.091 \ 0.834]^T, \bar{\Psi}_B = [1 \ 0]. \quad (8b)$$

Finally, an analysis of the residuals between the validation data and the identified LTI system was performed in order to obtain the characteristics of motor performance variation (v_i). This was done by performing a whiteness (independence) test of the residuals in order to establish whether v_i can be characterized by Gaussian white noise, and the mean and variance characteristics for each subject [13]. The whiteness test was performed with a 95% confidence interval and the validation data-set for each subject contained 50 samples, such that the validation criterion was 0.277. This criterion represents the maximum auto-correlation permitted between the residuals in order to accept the hypothesis that the residuals have a Gaussian distribution. The resultant normalized autocorrelations from the analysis of residuals were 0.1495 and 0.227 for subject A and B respectively, both smaller than the validation criterion. Therefore, it is concluded with 95% confidence that v_i has a Gaussian distribution. The individual v_i characteristics for each subject are presented in Table II.

TABLE II

MEAN AND STANDARD DEVIATION OF RESIDUALS OBTAINED FROM WHITENESS TEST.

Subject	Mean (μ)	Standard deviation (σ)
A	0	16.81
B	0	22.36

E. Simulations

The identified model of the individual subject behavior (subject A and subject B above) is numerically simulated and

the output was compared to an independently obtained validation data-set for the respective subjects. The experimental data-set for validation was generated for the same forward reaching task as the identification data-set. However, in this case the synergy was changed at each iteration according to:

$$\theta_i = 0.8 + \frac{i}{125}, \quad (9)$$

where i represents the i th iteration of the task. The synergy range studied, $\theta_{min} = 0.8$ and $\theta_{max} = 2.4$, was informed by preliminary results in [14]. Performance of the task for a given iteration was measured by the objective function (1). Figures 6 and 7 present the experimental data and simulation results for subjects A and B respectively.

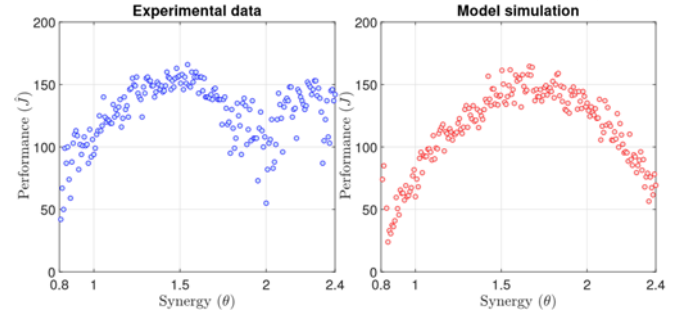


Fig. 6. Subject A experimental and model simulation synergy sweep performance response.

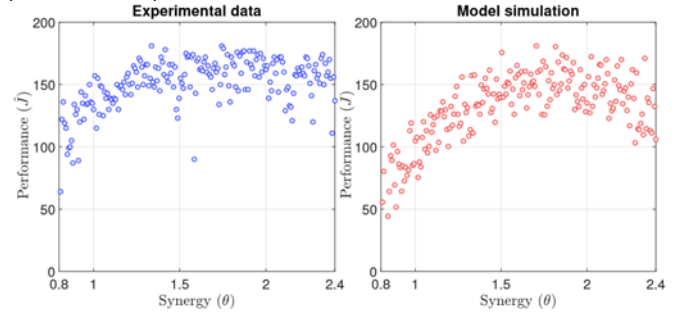


Fig. 7. Subject B experimental and model simulation synergy sweep performance response.

It can be seen from Figures 6 and 7 that the structure of the model is able to qualitatively capture the common features of motor preference (the shape of the non-linear I-SSO map) and adaption (the transient behavior) across the population, as well as human variation given the identified parameters $\bar{\lambda}$, $\bar{\Phi}$, $\bar{\Gamma}$, $\bar{\Psi}$, \bar{v} depend on individuals. In the validation data for subject A, presented in Figure 6, an increase in performance can be observed for $\theta > 2$. This behavior may be attributed to the subject changing their motor strategy in order to improve their performance for that synergy range. It was anecdotally observed, however, that this change in strategy relied on upper body and shoulder compensation motion. This highlights a limitation of the chosen measure of performance (1), as it does not capture compensation motion or metabolic effort. Nonetheless, even with such diverse human variation, both individually and across the population, the model adequately captures both the underlying common behavior of a population and individual behavior.

With the existence of a personalized interface parameter optimal value and the common model structure identified from experimental results, a grey-box based on-line

optimization technique [17], [18] can be naturally linked to the kinematic synergies personalization problem in HPIs. This technique is able to find the optimal personalized solution to the interface parameter to performance problem in the presence of human variation. Differing from black-box on-line optimization techniques with personalized tuning of parameters and personalized convergence performance, the grey-box on-line optimization technique utilizes the common model structure to obtain a uniformly convergent performance among the population with tuning parameters that are less sensitive to human variation.

III. HUMAN-PROSTHESIS INTERFACE PERSONALIZATION ALGORITHM

The interface personalization algorithm is discussed in this section. It is adapted from [17] and [18] for the HPI application. The major change is that the current setting is in the iteration domain due to the event-driven iterative nature of the problem. Figure 8 presents the diagram of the proposed framework for personalization of human-prosthesis interfaces.

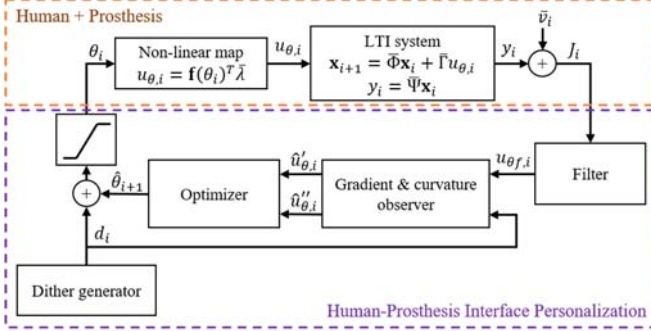


Fig. 8. General overview of the proposed framework for personalization of human-prosthesis interfaces.

The algorithms in [17] and [18] require that certain conditions are satisfied to ensure that the parameter θ will converge close to the optimal θ^* . A summary of these conditions is presented herein.

Condition 1. *There exists an extremum θ^* in the non-linear steady-state map $J(\theta)$ and the map is twice continuously differentiable [17, Assumption 2].*

Condition 2. *The relative degree of the LTI dynamic system is known [17, Condition 6].*

Condition 3. *The serial combination of the LTI System and the Filter (Figure 8, block A) is minimum phase [17, Condition 6].*

Condition 4. *Persistency of excitation (PE) is satisfied for parameter estimation.*

Assumption 1 ensures that Condition 1 is satisfied. Section II identified that the normalized LTI system has a relative degree one. Thus Condition 2 is satisfied. Given that the system (4) represents human motor adaptation behaviour, it indicates that the matrix Φ is stable, thus satisfying Condition 3. Persistency of excitation is a common condition required in adaptive systems. Condition 4 can be satisfied by introducing a known dither (perturbation) signal that excites the parameters that need to be identified.

A. Filter

The role of the filter is to extract the information of nonlinear map u_θ from the measured task performance J , which contains performance variability and measurement noise. It is the component that ensures that the tuning parameters are independent of individual motor adaptation dynamics.

Conditions 2 and 3 are needed for filter design since the objective of the filter is to invert the dynamics of the LTI system. Ideally, this allows the estimation of the non-linear map to be insensitive to the individual's learning behavior. With these conditions satisfied, then the stability of the closed loop can be ensured and an appropriate filter for the LTI system can be designed. In this work, a band-pass filter is used in order to maintain causality. Let the dither signal frequency range be $[\omega_o, n\omega_o]$, then the band-pass filter can be represented in state-space as follows.

$$\mathbf{w}_{i+1} = \Phi_f(\omega_o, n\omega_o)\mathbf{w}_i + \Gamma_f J_i, \quad (10a)$$

$$u_{\theta f,i} = \Psi_f(\omega_o, n\omega_o)\mathbf{w}_i, \quad (10b)$$

where $\mathbf{w} \in \mathbb{R}^{n_f}$ is the state of the filter. The order of the filter $n_f > 0$ is dependent on the LTI system. As the LTI system identified from the experiments has relative degree one, a second order filter is used with $n_f = 2$. Hence, the matrix $\Phi_f(\omega_o, n\omega_o)$ is in $\mathbb{R}^{2 \times 2}$, the matrix Γ_f in \mathbb{R}^2 , and the matrix $\Psi_f(\omega_o, n\omega_o)$ in $\mathbb{R}^{1 \times 2}$.

B. Gradient and Curvature Observer

This component estimates the gradient and curvature information from the non-linear map u_θ in order to find θ^* , provided that Condition 4 is satisfied. There are multiple methods for performing these estimates, such as demodulation [25] and observer based [17].

In this work, a discrete version of the Luenberger observer method presented in [18] is used. The observer takes the following form

$$\hat{u}_{\theta f,i} = \Psi_o \hat{\mathbf{z}}_i \quad (11a)$$

$$\hat{\mathbf{z}}_{i+1} = \omega_o \Phi_o \hat{\mathbf{z}}_i + \omega_o \mathbf{L}(u_{\theta f,i} - \hat{u}_{\theta f,i}) \quad (11b)$$

where $\mathbf{L} \in \mathbb{R}^5$ is the observer gain which is designed such that $\Phi_o - \mathbf{L}\Psi_o$ is stable, so that the estimated gradient and curvature will converge to the true values. The matrices of the observer take the following form as in [18]:

$$\Phi_o = \begin{bmatrix} 0 & 0 & 0 & 0 & 0 \\ 0 & 0 & 1 & 0 & 0 \\ 0 & -1 & 0 & 0 & 0 \\ 0 & 0 & 0 & 0 & 2 \\ 0 & 0 & 0 & -2 & 0 \end{bmatrix}, \quad \Psi_o = \begin{bmatrix} 1 \\ 1 \\ 0 \\ 0 \\ -0.25 \end{bmatrix}. \quad (12)$$

Then u'_θ and u''_θ can be estimated by demodulating the states $\hat{\mathbf{z}}$, such that

$$\hat{u}'_{\theta,i} = \frac{1}{a} \Psi' \hat{\mathbf{z}}_i, \quad \Psi' = [0 \quad \mathcal{S}_1 \quad \mathcal{C}_1 \quad 0 \quad 0], \quad (13a)$$

$$\hat{u}''_{\theta,i} = \frac{1}{a^2} \Psi'' \hat{\mathbf{z}}_i, \quad \Psi'' = [0 \quad 0 \quad 0 \quad \mathcal{S}_2 \quad \mathcal{C}_2], \quad (13b)$$

where $S_n = \sin(n\omega_o i)$ and $C_n = \cos(n\omega_o i)$, $n = 1, 2$ are the dithers needed for estimation, and $i > 0$ is the iteration operator. By using S_n , C_n , and standard averaging techniques [26, Chapter 10], the output of the observer will converge close to the gradient and curvature of the non-linear map.

Remark 4. *It is important to note that curvature estimation is on a faster time-scale than gradient due to Condition 4. Hence the demodulation dither signals S_2 and C_2 operate on a $2\omega_o$ frequency. Given the iterative nature of the system, care must be taken when selecting ω_o to avoid issues such as aliasing.*

C. Optimizer

Once the gradient and curvature of the non-linear map are estimated, they can be used in an optimizer to find the optimal θ^* . With consideration of human variations, the optimizer is designed such that it can achieve uniform convergence performance, which is independent to the shape of the nonlinear map $u_\theta(\cdot)$.

A widely used optimizer is gradient-ascent, see for example [27], [15] and references therein. The gradient-ascent method with a fixed step size is simple to implement, but the convergence speed is determined by the shape of the non-linear map (given by $\bar{\lambda}$ in this work). In order to achieve uniform convergence speed across individuals, the derivative based optimizer employed in this paper switches between a gradient-ascent and a Newton-like approach. The reason to add the Newton-like approach is two-fold. First, the faster convergence speed. Second, its performance being less sensitive to the shape of the non-linear map. Although, the shape of the nonlinear map varies over the population, convergence speed of the proposed HPI personalization algorithm is insensitive to this variation.

Assumption 1, particularly equation (3b), is needed to ensure that the Newton-like optimizer is applicable. However, this can only be satisfied locally as shown from experimental results in [14]. This local region is usually smaller than the region where gradient-descent can converge. Thus the Newton-like optimizer must operate within the region in which equation 3b is satisfied. The gradient-descent optimizer operates outside that region. As such, the following switching mechanism is used.

$$\hat{\theta}_{i+1} = \hat{\theta}_i + k\omega_o\Delta_i \quad (14a)$$

$$\Delta_i = \begin{cases} -\frac{\hat{u}'_{\theta,i}}{\hat{u}''_{\theta,i}} & \|\hat{u}'_{\theta,i}\| < -\varepsilon\hat{u}''_{\theta,i}, \\ \hat{u}'_{\theta,i} & \text{otherwise,} \end{cases} \quad (14b)$$

where $\varepsilon > 0$ determines the size of the region where a Newton step is employed, and $k > 0$ is the optimizer gain. The condition $\|\hat{u}'_{\theta,i}\| < -\varepsilon\hat{u}''_{\theta,i}$ serves two purposes. First, to ensure that when the Newton-like optimizer is used, equation 3b of Assumption 1 is satisfied. Second, to avoid numerical issues arising when $\hat{u}''_{\theta,i}$ is close to zero.

Remark 5. *An important consideration with the tuning of this algorithm is the time-scale separation between the observer and the synergy (θ) rate of change. The change in θ needs to*

be sufficiently slow to ensure that the observer provides relatively accurate estimation of the gradient and curvature. By carefully tuning the optimizer gain (k), such time-scale separation can be achieved. The tuning guideline can be found in [18].

D. Dither Generator

In order to be able to estimate the gradient and curvature of the non-linear map $u_\theta(\cdot)$, as a standard requirement in parameter identification, Condition 4 is needed. This is done by perturbing the system with a known dither vector [12]. Since gradient and curvature need to be estimated, two different dither signals are required.

Let the estimation frequency to be used for gradient be ω_o . In this work, a sinusoidal dither generator is used, leading to the following dither vector:

$$\mathbf{d} = [a\mathcal{S}_1 \quad a\mathcal{S}_2]^T \quad (15)$$

where $a > 0$ is the dither amplitude.

Remark 6. *It has been found that high variability can impair human motor learning [28], so care must be taken to ensure the dither amplitude is not too large.*

E. Personalization algorithm implementation with simulated humans

With the multiple conditions that need to be satisfied for the application and tuning of the algorithm, it is desirable to test it on simulated humans before it is applied to human-in-the-loop applications. This simulation can be performed through the identified motor preference and adaptation model presented in the previous section. Here the kinematic synergies personalization simulation results for the two subjects previously modeled are presented.

Tuning of the algorithm was performed by first selecting the dither frequency ω_o and amplitude a as they play an important role to ensure convergence. Considering the application, it is desirable to achieve convergence of algorithm within the time for a prosthesis fitting and training session. From previous experiments with reaching tasks, it was found that 100 to 200 iterations are acceptable for a training session as this number of iterations take 30 to 60 minutes to perform. In the sequel, the dither frequency needed is selected as $\omega_o = \pi/4$. Given that the system is of relative degree one, a second order bandpass Q-filter was chosen. The following parameters were used for its design: $H = 0.5$ and $Q = 5.0$.

The choice of a presents one of the first challenges for a human-in-the-loop system (see Remark 6). From the point of view of the human, it would be difficult to learn to use a device that is constantly and unpredictably changing its behavior. Furthermore, the choice of a will affect the estimator. From previous experiments, it was found that $a \leq 0.05$ is well received by subjects, thus a dither amplitude of $a = 0.02$ was chosen. Finally, the optimizer parameters were chosen by evaluating the system response with a range

of optimizer gain k values. Final algorithm parameters were: observer gain

$\mathbf{L} = [1.5 \ 0.25 \ 0.25 \ 2.0 \ -2.0]$, $\varepsilon = 0.1$, $k = 0.05$, and output noise v variance σ_v as identified for each subject.

The algorithm the authors previously presented in [15] was also implemented. Such algorithm uses a “black-box” online optimization technique without exploring the transient behaviour of human learning. Hence it suffers the disadvantage that the tuning parameters are sensitive to person-to-person variation. In order to demonstrate such sensitivity, the same tuning parameters are used for both individuals. Algorithm parameters a and w were equivalent to those used for the proposed algorithm, while k was modified to $k = 0.005$ as required by the different optimizer. Simulation results for the algorithm in [15] are presented in Figure 9, where performance and synergy for the two subjects is shown.

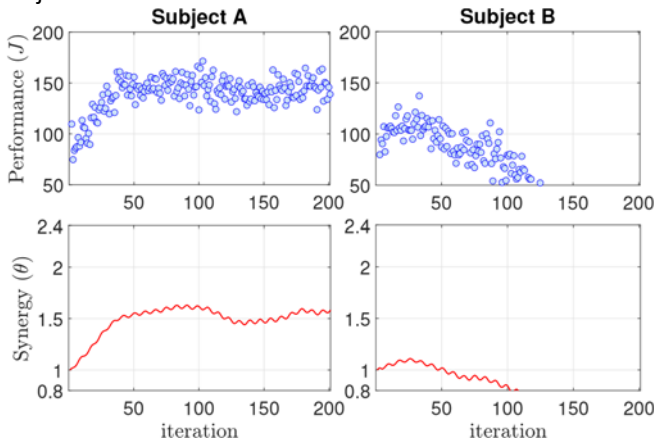


Fig. 9. Previous algorithm ([15]) simulation results for performance and synergy for the two modelled subjects. Top plots show performance across iterations while bottom plots show synergy across iterations. The algorithm fails to identify the optimal synergy for subject B.

It is clear in Figure 9 from the decreasing performance of subject B, that the previous algorithm [15] failed to identify the synergy for this subject when the same algorithm parameter tuning was used for both subjects. This is due to the tuning parameters of this algorithm being dependent on each individual.

Simulation results for the algorithm proposed in this paper are presented in Figure 10, where performance (J) and synergy (θ) of the two modeled subjects is shown.

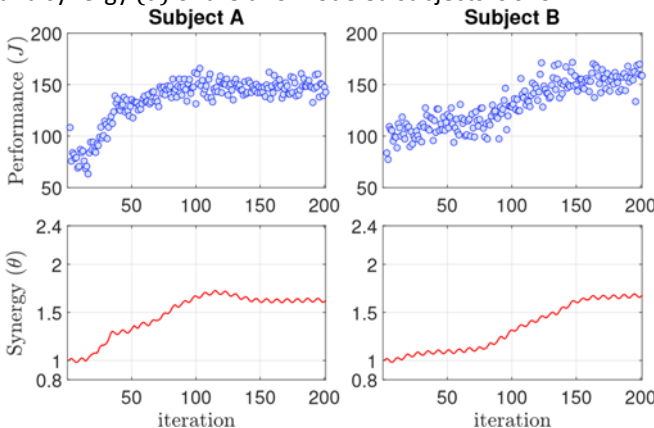


Fig. 10. Proposed algorithm simulation results for performance and synergy for the two modelled subjects. The top plots show performance across

iterations while the bottom plots show synergy across iterations. The algorithm successfully identifies the optimal synergy for both subjects.

As can be observed in Figure 10, the proposed algorithm updates the synergy over iterations of the task until the maximum performance (as defined by the identified map used for simulation) is reached. Thus, the proposed algorithm was able to successfully identify the synergy for the two modeled subjects using the same tuning parameters. This demonstrates the capability of the proposed algorithm to handle individual motor preference and adaptation dynamics without the need for individual tuning.

IV. SYNERGISTIC PROSTHESIS ADAPTATION EXPERIMENT

A human-in-the-loop experiment in a Virtual Reality environment was designed to emulate amputation and prosthesis use in able-bodied subjects. The implementation of the proposed personalization algorithm to a virtual synergistic prosthetic elbow device on human subjects is demonstrated.

A. Experiment description

The experiment required subjects to perform a center-out forward reaching task in a Virtual Reality (VR) environment. Transhumeral amputation was simulated by tracking only the motion of the subject’s dominant upper arm, as shown in Figure 11.A, which determined the motion of the virtual residual limb. A virtual synergistic elbow prosthetic device was used for the task. The task required subjects to reach between two targets, as shown in Figure 11.B, whose position was maintained constant throughout the experiment. A scalar linear kinematic synergy related to shoulder flexion/extension was chosen for the HPI parameterization, given by

$$\dot{q}_p = \theta \dot{q}_r. \quad (16)$$

The subscripts r and p represent residual and prosthetic limb respectively. \dot{q}_r is the subject’s shoulder flexion/extension angular velocity. \dot{q}_p is the angular velocity for the prosthetic elbow. And $\theta \in [0.8, 2.4]$ the synergy that parameterizes the human-prosthesis interface, which is to be identified. An initial synergy $\theta_0 = 1.0$ was chosen for the task.

Performance of the task for a given iteration was determined by the objective function presented in equation (1), which is related to reaching accuracy and time. The performance score was presented to subjects after each repetition of the task. This was done in order to control the variable that relates to the difference between an individual’s measure of performance and our designed function. The reaching-time was limited to 3 seconds. Failed attempts that did not reach within this time were not considered for algorithm update and had to be repeated. The first dither period was used to initialize the different filters and components of the algorithm, therefore no synergy update was performed during this period. The same algorithm tuning as in the simulation implementation was used.

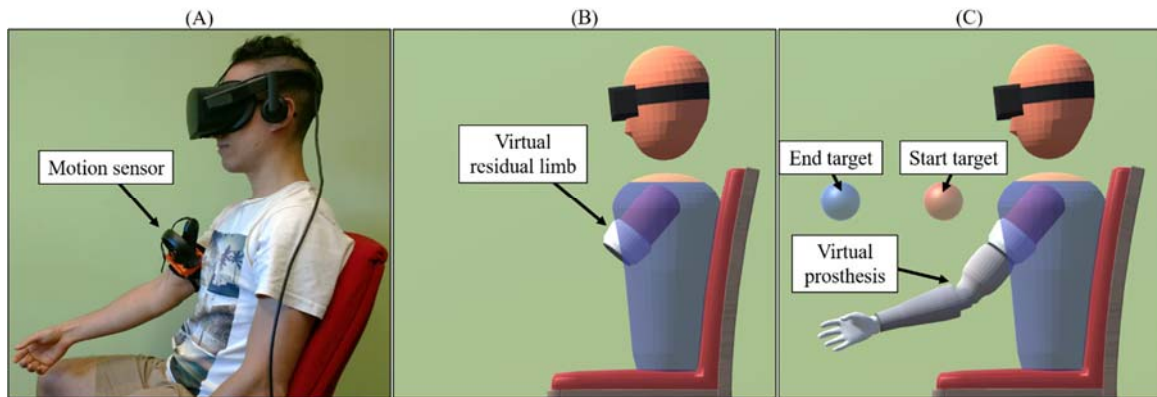


Fig. 11. Virtual Reality (VR) experimental platform set-up. (A) Subject position and motor sensor placing. The motion sensor is placed on the subjects upper-arm to emulate transhumeral amputation. (B) Virtually amputated subject in VR environment. The virtual residual limb tracks the subject's upper-arm as per the motion sensor. (C) Subject's avatar with virtual prosthesis. The lower-arm is replaced by a prosthetic device. The task requires subjects to reach between the start (red) and end (blue) targets.

B. Experimental protocol

The experiment was performed on 12 able-bodied subjects, 7 female and 5 male. The mean age and range were 30 and 19-68 respectively. Subjects received instructions on how to perform the task and performed the motion with their dominant arm before going into VR. First, the position of the sensor was calibrated and the virtual arm was fitted to resemble their actual limb in size as close as possible as with fitting of a prosthetic device. Subjects received instructions about the task and scoring system in VR and were allowed 5 practice iterations with no time limit. Subjects had to perform the task for 150 iterations, receiving 1 minute rest every 25 iterations to minimize upper arm fatigue, and received 5 minutes rest outside VR after the 75th iteration in order to reduce VR induced fatigue. Subjects' experience with VR environments ranged from no previous experience to casual users for gaming. No noticeable difference in performance of the task was noticed among subjects with different exposure to VR. The procedure was approved by the University of Melbourne's Ethical Review Board under project number 1750711.1.

C. Hardware set-up and data gathering

The VR experiment platform was developed on an Oculus Rift headset with the application developed in Unity3D. The experiment was run on an Intel Core i7-7700HQ processor at 3.8GHz, with 16GB RAM, and an NVIDIA GeForce GTX 1070 video card with 8GB GDDR5. The Oculus Rift set-up included 3 tracking sensors, two placed in the front corners of the room and one in a back corner, and one Oculus Touch controller. Data gathering and VR update were performed at 90Hz. The subject's shoulder rotation and angular velocity in 3 DOF, the rotation and angular velocity of the virtual prosthetic elbow, and hand position and velocity in 3D space were gathered.

D. Experimental results and discussion

Experimental results are presented in Figures 12 and 13, where performance and synergy across iterations are shown for all subjects respectively. It can be observed in Figure 12 that performance steady-state was reached under 50

iterations on average, which was achieved uniformly across most subjects, highlighting the uniform performance achieved by the algorithm. As has been previously identified, the synergy-performance map can be quite flat. This can be seen for instance in subject (G), where a large change in synergy lead to a small change in performance. However, the Newton-like optimizer allows the algorithm to adapt its step-size to address this. A wide variety of capabilities are observed among the different subjects which is expected of human behavior. Multiple different performance steady-states with different best synergies can be seen across subjects. This further highlights individuality, and the importance and need of personalization in human-prosthesis interfaces. Motor performance variation (v) is another clear indicator of individuality, with different people having different levels of variability. In subjects with small identified v , very clear performance steady-state and convergence of synergy are observed, such as subjects (H) and (L). On the other hand, in subjects with higher v , the performance steady-state is not as clear and a wider drift in synergy is observed, such as with subjects (F) and (K). This highlights kinematic synergies inherently have sensitivity to individual motor performance variation and noise. In light of the observed diversity in behavior, the personalization algorithm was capable of adapting the synergy to allow all subjects to significantly improve their performance while using the same algorithm tuning across all subjects. This demonstrates the advantages of the proposed algorithm for personalization of synergistic HPIs.

Another important observation was that subjects changed their arm motor behavior with the synergy. The initial (suboptimal) synergy value required subjects to perform compensation movements with their upper body and shoulder in order to achieve the task, as seen in Figure 14.A. This type of compensation motion is common among prosthesis users [29]. Figure 14 shows the comparison between a subject's reach position during the first and last 10 iterations. The compensation required by subjects to perform the task was observed to gradually diminish as the personalization algorithm gradually approximated the synergy setting to the optimal one for the individual.

This reduction in compensation motion was also anecdotally reported by subjects, who stated that the

motion they had to perform by the last few iterations felt more natural compared to the initial ones. This may be an additional positive effect of personalizing the synergistic HPI, as compensation is a significant issue for prosthesis users [1], [29]. Quantifying compensation motion as part of the measure of performance may prove to be advantageous to the personalization of kinematic synergies in HPIs given that reducing the compensation motion required by prosthesis users to perform a task may improve the ease of use and usability of these devices.

V. CONCLUSION

In this paper, an algorithm for on-line personalization of kinematic synergies for Human-Prosthesis Interfaces whose tuning is independent of individual motor behavior and learning was proposed. Moreover, the algorithm is able to achieve uniform convergence performance across the population. In order to achieve this, the algorithm takes advantage of common motor preference and adaptation behavior observed experimentally in a group of individuals using an emulated synergistic upper limb prosthetic device. This motor behavior was formally characterized with a model structure which captures the common behavior across a population.

The application of the proposed personalization algorithm was undertaken in a virtual reality environment with able-bodied subjects by emulating amputation and prosthesis use. The algorithm was capable of adapting the synergy to allow all subjects to improve their performance while it was anecdotally observed that it reduced the compensation motion required by individuals to perform the task, despite the demonstrated person-to-person variations. Convergence performance of the algorithm was uniform across subjects using the same parameter tuning, avoiding the need for manual tuning for each individual.

Further work will look into quantifying the effects of prosthesis interface personalization on compensation motion and the effects of the choice of objective function for personalization on motor behavior and performance, the application of the algorithm to other interface modalities, and the development of a practical implementation of the proposed personalization framework on a prosthetic device with wearable motion sensors.

REFERENCES

- [1] E. A. Biddiss and T. T. Chau, "Upper limb prosthesis use and abandonment: A survey of the last 25 years," *Prosthet. Orthot. Int.*, vol. 31, no. 3, pp. 236–257, 2007.
- [2] A. Fougner, O. Stavadahl, P. J. Kyberd, Y. G. Losier, and P. A. Parker, "Control of Upper Limb Prostheses: Terminology and Proportional Myoelectric Control - A Review," *IEEE Trans. Neural Syst. Rehabil. Eng.*, vol. 20, no. 5, pp. 663–677, 2012.
- [3] N. A. Alshammary, D. A. Bennett, and M. Goldfarb, "Synergistic Elbow Control for a Myoelectric Transhumeral Prosthesis," *IEEE Trans. Neural Syst. Rehabil. Eng.*, vol. 26, no. 2, pp. 468–476, 2018.
- [4] G. L. Gottlieb, Q. Song, D. A. Hong, G. L. Almeida, and D. Corcos, "Coordinating movement at two joints: a principle of linear covariance," *J. Neurophysiol.*, vol. 75, no. 4, pp. 1760–1764, 1996.
- [5] F. Cordella, A. L. Ciancio, R. Sacchetti, A. Davalli, A. G. Cutti, E. Guglielmelli, and L. Zollo, "Literature Review on Needs of Upper Limb Prosthesis Users," *Front. Neurosci.*, vol. 10, may 2016.
- [6] M. Merad, E. de Montalivet, A. Touillet, N. Martinet, A. Roby-Brami, and N. Jarrasse, "Can We Achieve Intuitive Prosthetic Elbow Control Based on Healthy Upper Limb Motor Strategies?," *Front. Neurobot.*, vol. 12, 2018.
- [7] R. R. Kaliki, R. Davoodi, and G. E. Loeb, "Evaluation of a noninvasive command scheme for upper-limb prostheses in a virtual reality reach and grasp task," *IEEE Trans. Biomed. Eng.*, vol. 60, no. 3, pp. 792–802, 2013.
- [8] D. Blana, T. Kyriacou, J. M. Lambrecht, and E. K. Chadwick, "Feasibility of using combined EMG and kinematic signals for prosthesis control: A simulation study using a virtual reality environment," *J. Electromyogr. Kinesiol.*, vol. 29, pp. 21–27, 2016.
- [9] M. Merad, E. de Montalivet, A. Roby-Brami, and N. Jarrasse, "Intuitive prosthetic control using upper limb inter-joint coordinations and IMU-based shoulder angles measurement: A pilot study," in *Int. Conf. Intell. Robot. Syst.*, pp. 5677–5682, 2016.
- [10] A. Akhtar, N. Aghasadeghi, L. Hargrove, and T. Bretl, "Estimation of distal arm joint angles from EMG and shoulder orientation for transhumeral prostheses," *J. Electromyogr. Kinesiol.*, vol. 35, pp. 86–94, 2017.
- [11] M. Legrand, M. Merad, E. de Montalivet, A. Roby-Brami, and N. Jarrasse, "Movement-Based Control for Upper-Limb Prosthetics: Is the Regression Technique the Key to a Robust and Accurate Control?," *Front. Neurobot.*, vol. 12, 2018.
- [12] K. B. Ariyur and M. Krstic, *Real-Time Optimization by Extremum Seeking Control*. Springer, 2003.
- [13] I. D. Landau, R. Lozano, M. M'Saad, and A. Karimi, *Adaptive Control*. Springer, 2011.
- [14] R. Garcia-Rosas, D. Oetomo, C. Manzie, Y. Tan, and P. Choong, "On the Relationship Between Human Motor Control Performance and Kinematic Synergies in Upper Limb Prosthetics," in *Eng. Med. Biol. Conf.*, pp. 3194–3197, 2018.
- [15] R. Garcia-Rosas, Y. Tan, D. Oetomo, and C. Manzie, "On-line Synergy Identification for Personalized Active Arm Prosthesis: a Feasibility Study," in *Am. Control Conf.*, pp. 514–519, 2018.
- [16] S. Kumar, A. Mohammadi, N. Gans, and R. D. Gregg, "Automatic tuning of virtual constraint-based control algorithms for powered knee-ankle prostheses," in *Conf. Control Technol. Appl.*, pp. 812–818, 2017.
- [17] W. H. Moase and C. Manzie, "Fast extremum-seeking on Hammerstein plants," *IFAC Proc. Vol.*, vol. 44, no. 1, pp. 108–113, 2011.
- [18] W. H. Moase, C. Manzie, and M. J. Brear, "Newton-like extremumseeking part I: Theory," in *IEEE Conf. Decis. Control*, pp. 3839–3844, 2009.
- [19] M. A. Riley and M. T. Turvey, "Variability and determinism in motor behavior," *J. Mot. Behav.*, vol. 34, no. 2, pp. 99–125, 2002.
- [20] S. Cheng and P. N. Sabes, "Modeling Sensorimotor Learning with Linear Dynamical Systems," *Neural Comput.*, vol. 18, no. 4, pp. 760–793, 2006.
- [21] K. Wei and K. Kording, "Uncertainty of feedback and state estimation determines the speed of motor adaptation," *Front. Comput. Neurosci.*, 2010.
- [22] K. He, Y. Liang, F. Abdollahi, M. Fisher Bittmann, K. Kording, and K. Wei, "The Statistical Determinants of the Speed of Motor Learning," *PLOS Comput. Biol.*, vol. 12, no. 9, 2016.
- [23] S.-H. Zhou, D. Oetomo, Y. Tan, E. Burdet, and I. Mareels, "Modeling individual human motor behavior through model reference iterative learning control," *IEEE Trans. Biomed. Eng.*, vol. 59, no. 7, pp. 1892–901, 2012.
- [24] S.-H. Zhou, D. Oetomo, Y. Tan, E. Burdet, and I. Mareels, "Optimal learning gain selection in model reference iterative learning control algorithm for computational human motor systems," *Aust. Control Conf.*, pp. 338–344, 2011.
- [25] D. Nesi^c, Y. Tan, W. H. Moase, and C. Manzie, "A Unifying Approach to Extremum Seeking: Adaptive Schemes Based on Estimation of Derivatives," *IEEE Conf. Decis. Control*, pp. 4625–4630, 2010.
- [26] H. K. Khalil and J. Grizzle, *Nonlinear Systems*. Pearson, 3rd ed., 2002.
- [27] Y. Tan, D. Nesi^c, and I. Mareels, "On non-local stability properties of extremum seeking control," *Automatica*, 42, no. 6, pp. 889–903, 2006.
- [28] M. Cardis, M. Casadio, and R. Ranganathan, "High variability impairs motor learning regardless of whether it affects task performance," *J. Neurophysiol.*, 2017.
- [29] A. J. Metzger, A. W. Dromerick, R. J. Holley, and P. S. Lum, "Characterization of compensatory trunk movements during prosthetic upper limb reaching tasks," *Arch. Phys. Med. Rehabil.*, vol. 93, no. 11, pp. 2029–2034,

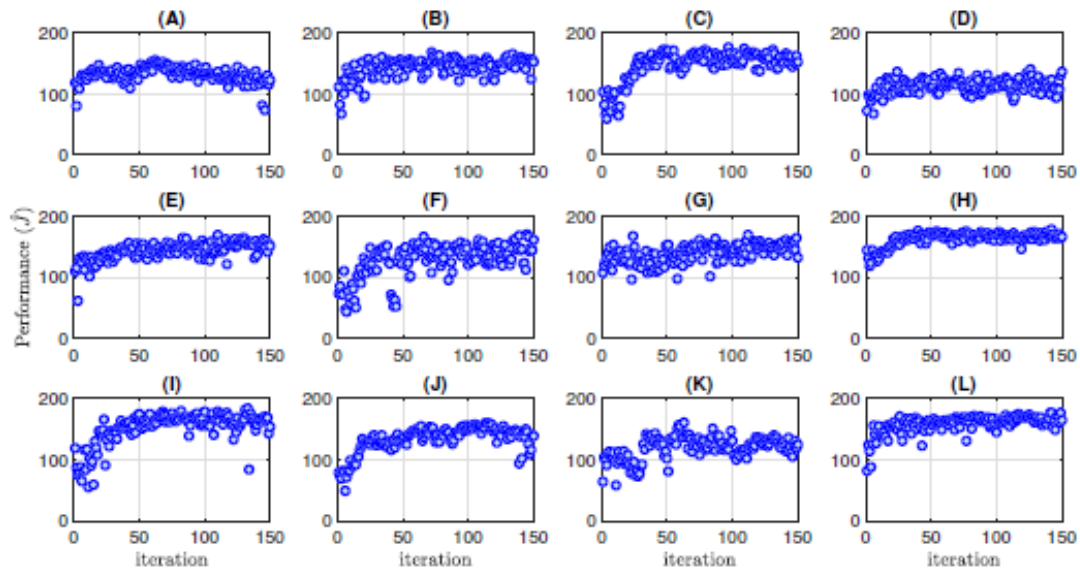


Fig. 12. Performance across iterations for all subjects in the experiment. A wide variety of capabilities can be observed among the different subjects, such as multiple different performance steady-states with different best synergies.

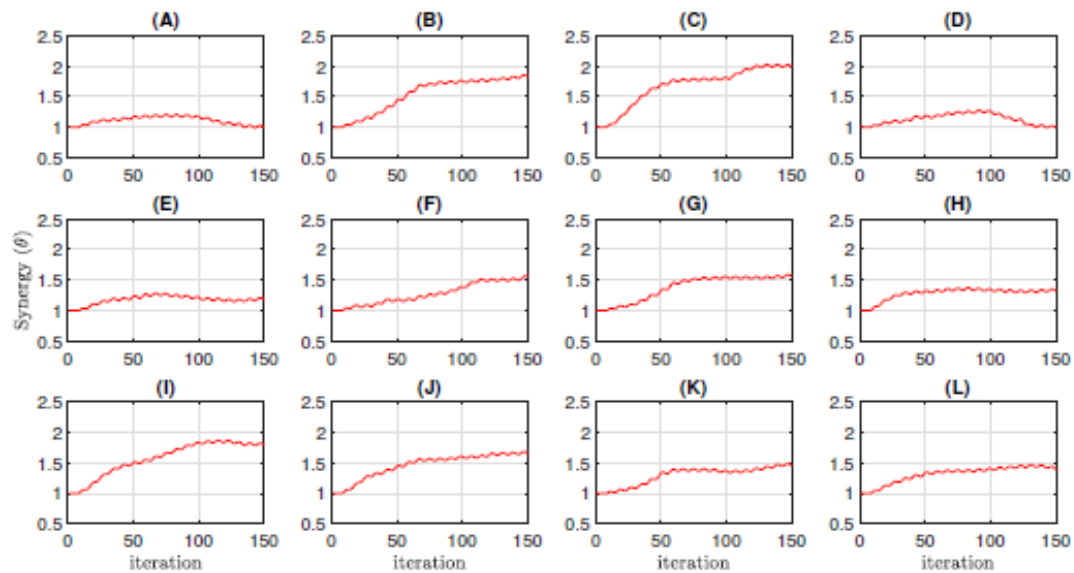


Fig. 13. Synergy across iterations for all subjects in the experiment. The personalization algorithm was capable of adapting the synergy to allow all subjects to significantly improve their performance while using the same algorithm tuning across all subjects.

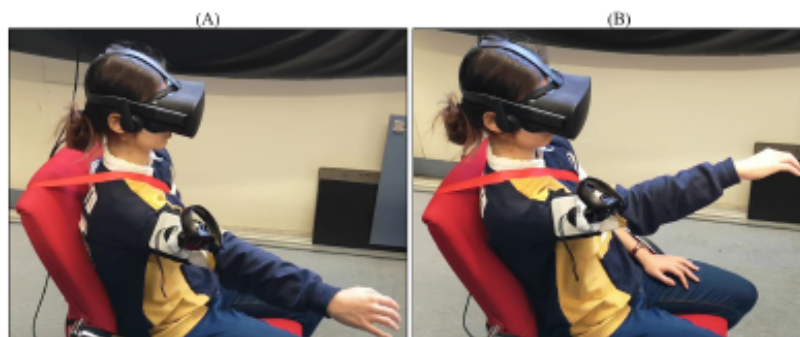


Fig. 14. Motor behavior changes with synergy for a representative subject, showing arm position at end of reaching task. (A) Sub-optimal synergy (first 10 iterations) causes subject to perform compensation movements with their upper body and shoulder. (B) Near-optimal synergy (last 10 iterations) allows subject to perform natural arm motion and minimize compensation motion.